Supporting Information

Unidirectional Transport Mechanism in an ATP Dependent Exporter

Yanyan Xu[1,2], Anna Seelig[2,*], and Simon Bernèche[1,2,*]

[1] SIB Swiss Institute of Bioinformatics, Biozentrum, University of Basel, Klingelbergstrasse 50/70, CH-4056 Basel, Switzerland
[2] Biozentrum, University of Basel, Klingelbergstrasse 50/70, CH-4056 Basel, Switzerland

[*]Correspondence to: anna.seelig@unibas.ch, simon.berneche@sib.swiss

Outward-closed and outward-open conformations of TMD

Helices 1 and 6 were subdivided in 3 segments. The rotation angle formed by the two first segments ("u" and "m") of each helix is analyzed. Rotation angle u-m is the rotation angle of segment "u" around the axis of segment "m" relative to the X-ray structure. For a given frame, the rotation angle was determined as follow: 1) Alignment of segment "m" to the X-ray structure; 2) Calculation of the projection of vector **u** on the plane normal to vector **m**; 3) Calculation of the angle between this projection and that of the X-ray structure.

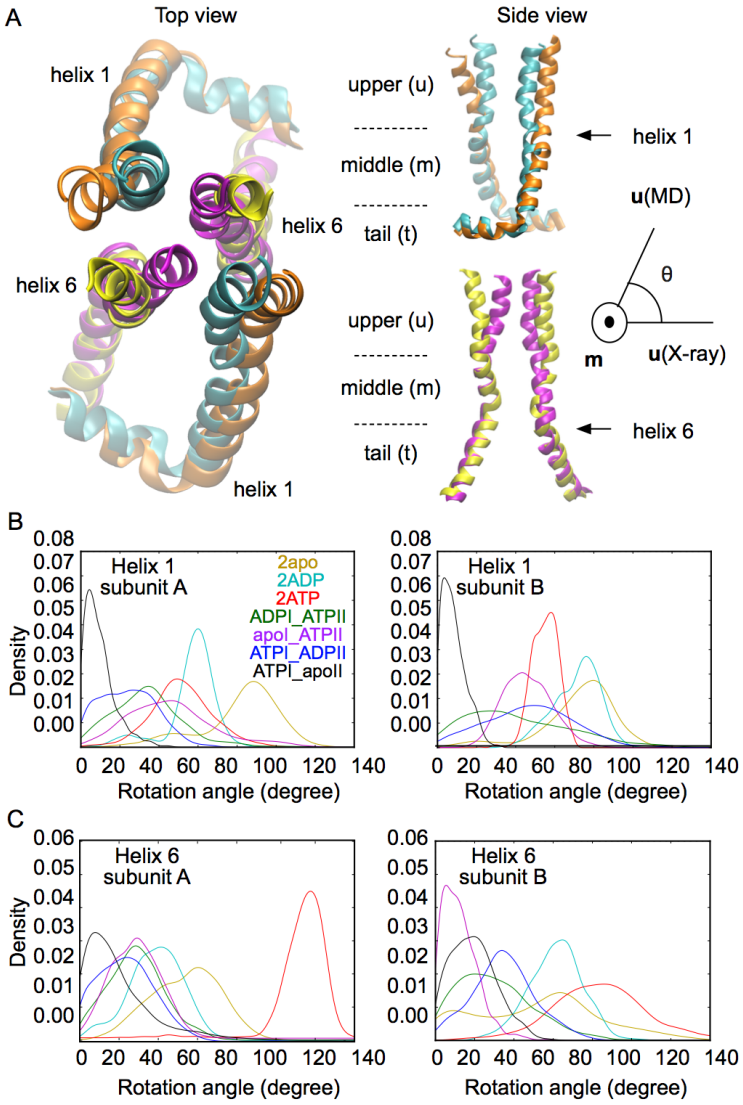

Figure S1. Rotation of helix 1 and helix 6 characterizes the two different TMD conformations. A: Top view and side view of helix 1 and helix 6 in the two different TMD conformations. The scheme illustrates the projection of segment "u" on the plane normal to segment "m". B, C: Density histograms of the rotation angle of helix 1 (B) and helix 6 (C) for different nucleotide occupancy states. Higher rotation angles are observed in the symmetric cases in comparison to the asymmetric cases in both helix 1 and helix 6.

Distribution of possible ligands for allocrite coordination and transport

As observed for Pgp[1], H-bond donor groups that could interact with allocrites, which typically carry H-bond acceptor groups, are more concentrated at the membrane-cytosol interface (Figure S2C). These H-bond donor groups could play a key role in allocrite recruitment. Near the center of the membrane, residues Glu288 could facilitate the flopping of cationic allocrites from the intracellular to the extracellular leaflet (Figure S2D). Contrariwise, an anionic molecule might be retained in the intracellular part of the protein due to its repulsion by the two Glu288 residues, potentially explaining the failure of the pump in the presence of anionic amphiphiles (P. Äänismaa, A. Beck, R. Müller, and A. Seelig, in preparation).

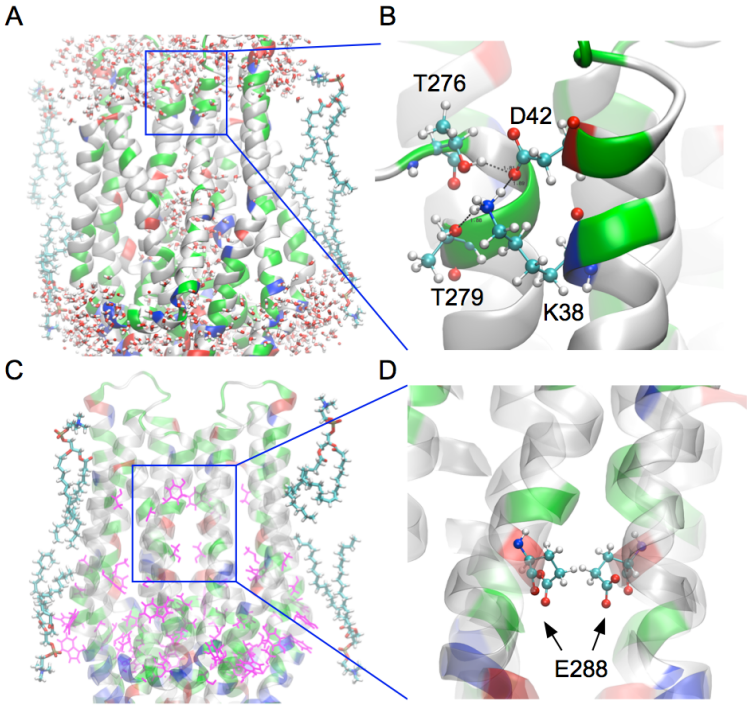

Figure S2. Representation of the TMD in the outward-closed conformation (2ATP occupancy state). A: Water molecules in the vicinity of the TMD concentrate at the intracellular leaflet, with only a few at the extracellular leaflet. B: Close-up view of the top of the hydrophobic bundle formed by helices 1 and 6 where two pairs of residues form H-bonds, K38-T279 and D42-T276. C: H-bond donors at the TMD level (highlighted in magenta) could possibly form H-bonds with allocrites. They concentrate on the intracellular side, with only a few on the extracellular side. D: Close-up view of the two E288 residues facing each other around the middle of the bilayer. Blue, positively charged residues; red, negatively charged residues; green, neutral non-hydrophobic residues; white, hydrophobic residues. Four lipid molecules (POPC), two from the extracellular leaflet, two from the intracellular leaflet are shown in panel A and C.

The transport cycle is not driven by association/dissociation of NBDs

The question as to whether NBDs completely dissociate or not during the transport cycle of ABC transporters has not been solved yet. In the absence of nucleotides (apo), X-ray structures of MsbA (Ref. 2) and Pgp (Ref. 3) show two completely separate NBDs, while that of CmABCB1 (Ref. 4) displays a state in which the NBDs are close to each other.

In our simulations of apo Pgp and apo Sav, the minimal separation of the two NBDs is around 15 Å (Figure S3A,B), much smaller than that displayed by the apo Pgp X-ray structure with the two NBDs separated by about 30 Å. Nevertheless, in the apo Sav simulation, the NBS binding distances (Figure S3C) and the interaction distances between helices 3 and 4 (Figure S6) show higher fluctuations than the other nucleotide occupancy states. Such flexibility could explain the various NBD separation distances observed in the X-ray structures. Another example is PglK, for which structures in the apo state are showing different NBD separations[5]. The different NBD separations of apo PglK were attributed to the type of detergent and crystal packing. This might also apply to the apo Pgp structure. The crystallographic unit cell of the Pgp crystal (PDB ID: 4m1m) reveals that the NBDs of proteins in adjacent unit cells form contacts (Figure S9). As a result, the interaction between NBDs of neighboring proteins may favor the dissociation of NBDs within a protein.

Could the flexibility provided by the apo state be essential to the transport cycle? Studies showed that this is not the case. Crosslinking the terminal ends of two NBDs of Pgp does not hinder transport[6], but rather favors transport[7]. Target molecular dynamic simulations of Sav demonstrated that the large conformational change in NBD obtained by pulling apart the two NBDs could not change the conformation of the TMDs[8]. Thus, the transport cycle seems unlikely to be driven by association and dissociation of the two NBDs.

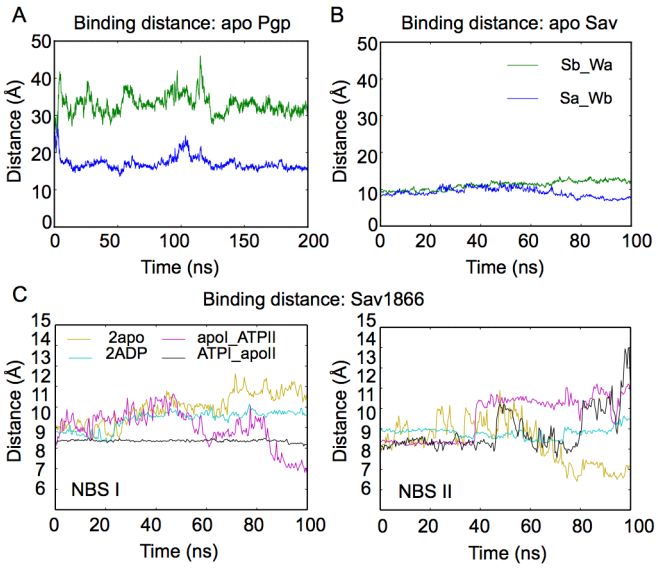

Figure S3. Time-series of binding distance between the center of mass of signature motif and the center of mass of Walker A for apo Pgp (A), apo Sav (B), and Sav in different nucleotide occupancy states (C).

Perturbation of NBS upon ATP hydrolysis

Figure S4 shows snapshots taken at t=100ns of the simulations in the 2ATP, ATPI_ADPII and ADPI_ATPII states. These snapshots reveal significant modifications in the network involving Lys483 in signature motif, Gln422, Asp423 and Asn424 in Q-loop, Glu473 and Arg474 in X-loop, Val117 in helix 3, and Gln208 in helix 4, suggesting a possible role in the coupling between NBD and TMD. In the 2ATP state, the two binding sites hold different conformations, principally arising from the asymmetry observed in the Sav X-ray structure[9]. Key residues at NBS I are highly solvated and do not form a stable interaction network, whereas they form a tight network in NBS II. In particular, Gln422 interacts with Mg^{2+}, which is bound between the beta and gamma phosphates of ATP; Asp423 forms a salt-bridge with Lys483; N424 forms a H-bond with Arg474. At NBS I, the other Arg474 forms a H-bond with the side chain of a Gln208, which itself form a H-bond with Gln208 from the other subunit. In addition, in both subunits, another H-bond is formed between Glu473 and Val117 (Figure S4B).

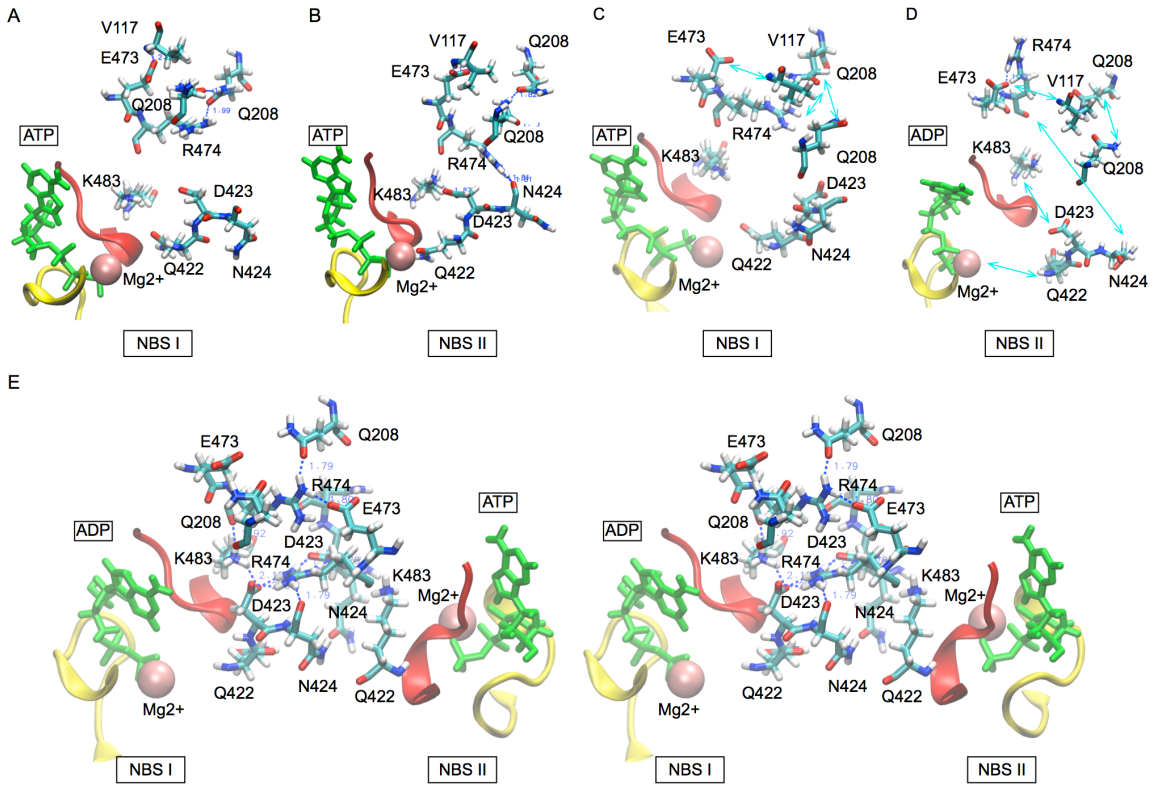

Figure S4. Reorganization of NBD upon ATP hydrolysis. A-E: Simulation snapshots taken at t=100ns are shown for different nucleotide occupancy states. The two NBSs are shown separately to highlight their asymmetry in 2ATP (A: NBS I. B: NBS II) and ATPI_ADPII (C: NBS I. D: NBS II). In the case of ADPI_ATPII, the two NBS are shown together since they more closely interact with each other (E: stereo view of NBS I and NBS II). The perturbations induced by ATP hydrolysis reach the bottom of the TMDs and disrupt the Q208-Q208 interaction. Green, ATP or ADP; yellow, Walker A; red, Signature motif; pink, Mg^{2+}.

In the ATPI_ADPII state, the initially well-formed network in NBS II is severely disrupted, with the breakage of the following interactions: Mg^{2+}-Gln422, Asp423-Lys483, Asn424-Arg474, Val117-Glu473 and Gln208-Gln208 (Figure S4D). The other binding site, NBS I, is also influenced with the loss of the H-bonds linking Arg474 to Glu208 and Glu473 to Val117 (Figure S4C). This illustrates a possible communication between the two binding sites.

In the ADPI_ATPII state, more interactions between residues from the two binding sites are observed (See Figure S4E). Arg474 from NBS II interacts with Asp423 from both subunits as well as Asn424 from NBS I, while Arg474 from NBS I moves up to interact with Gln208 and Glu473 at NBS II. With such disruption, the H-bond between Gln208 from the two subunits is broken and Gln208 from NBS I turns to form a H-bond with Glu473.

Whereas the pre-hydrolysis state holds an outward-closed conformation, the MD simulations suggest that hydrolysis at one NBS could turn it into an outward-open conformation. Interestingly, this does not apply to the 2ADP state, suggesting that an outward-open conformation depends on an asymmetric occupancy of the NBSs. Superposition of structures extracted from the simulations shows that in asymmetric nucleotide binding states (ADPI_ATPII, ATPI_ADPII), the orientation of Arg474 from the two subunits differs (Figure S5). When both binding sites are occupied by ADP (2ADP), the Arg474 residues from the two subunits remain in similar orientation and lie in a symmetric position. It seems that the perturbations produced by ADP at both NBS allow for local reorganization of the two Arg474 that minimizes their repulsion without disturbing the tetra-helix bundle, thus favoring the outward-closed conformation of the TMD.

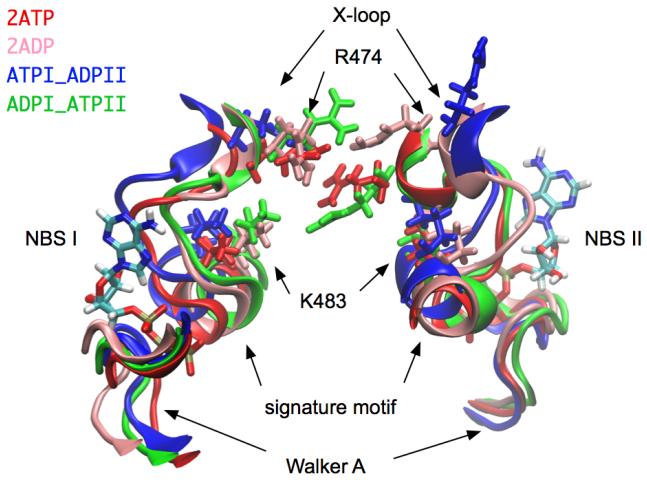

Figure S5. Asymmetry of nucleotide binding seems essential for triggering the movement of R474. Key residues are shown in a superposition of snapshots taken at t=100ns from simulations of Sav in the 2ATP, 2ADP, ATPI_ADPII and ADPI_ATPII states.

Interaction and conformation of helices 3 and 4

The interaction distances between helix 3 and helix 4 show important fluctuations in the case of the 2apo state (Figure S6).

The kink angle in helix 4 is larger in the cases of symmetric occupancy states of the NBSs (Figure S7). There is however an exception with subunit B in the 2apo state where the kink angle is smaller. This seems to be due to an unusually small NBS binding distance attributed to a deformed Walker A (Figure S3).

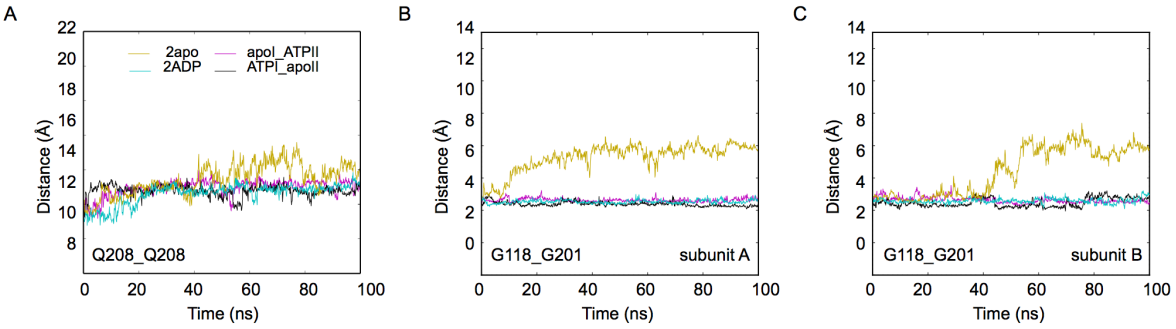

Figure S6. Time-series of distances between the center-of-mass of the backbone of the two Gln208 residues (A), of Gly118 and Gly201 in subunit A (B) or subunit B (C) for the 2apo, 2ADP, apoI_ATPII and ATPI_apoII cases.

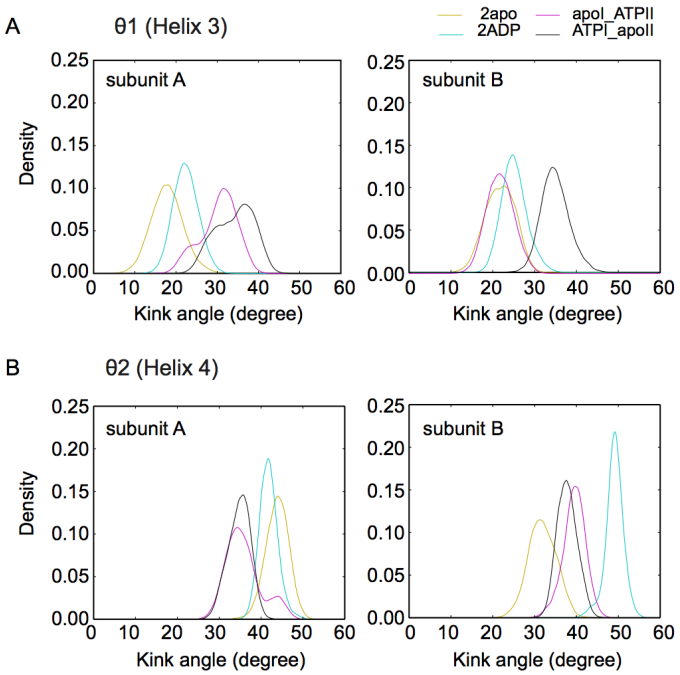

Figure S7. Density histogram of the kink angle for different nucleotide occupancy states (A: θ1 in helix 3. B: θ2 in helix 4).

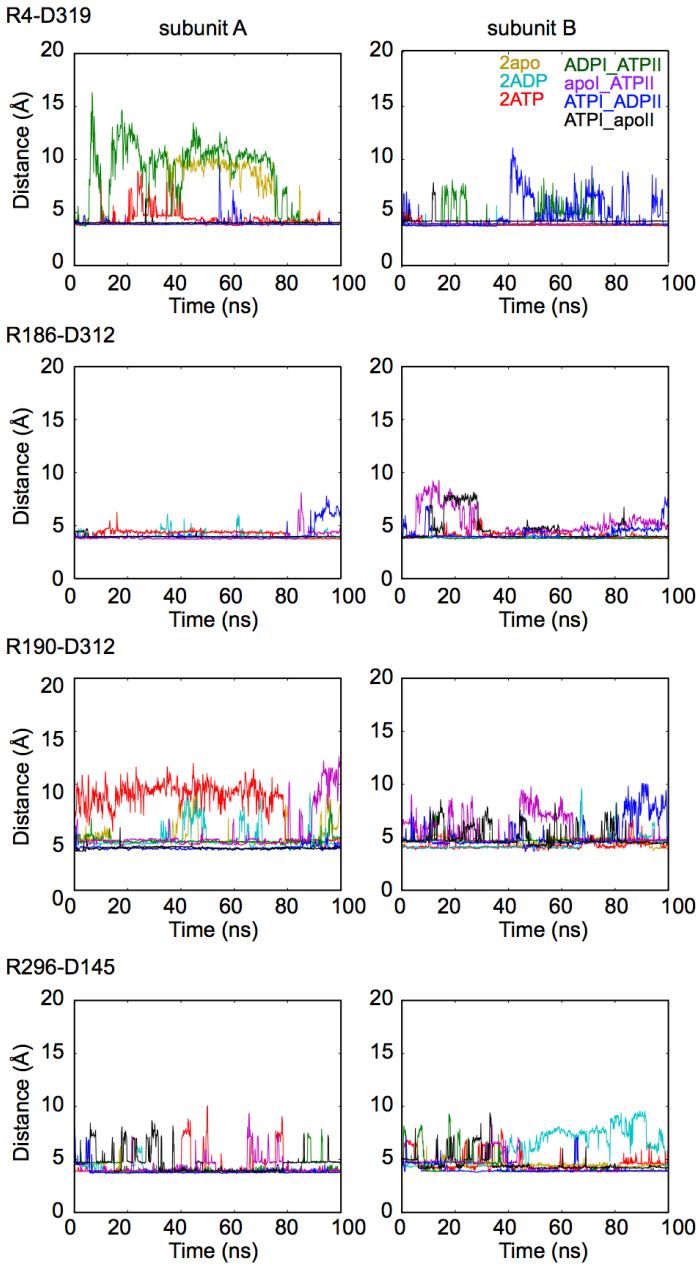

Figure S8. Time-series for the different salt-bridges that form a network among helices 1, 3, 4, and 6.

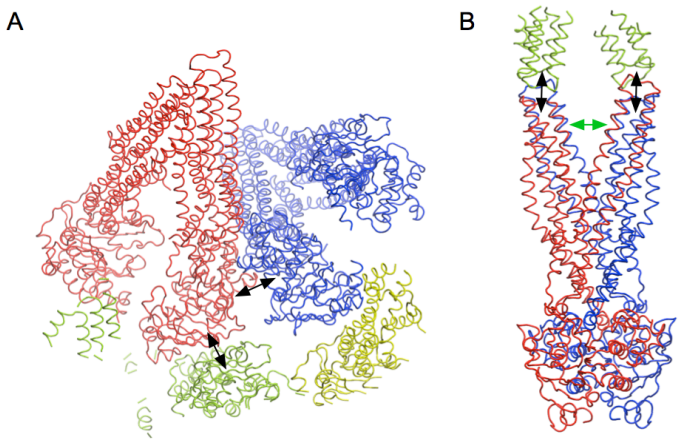

Figure S9. Crystal packing of Pgp and Sav structures. A: mouse Pgp, PDB ID: 4m1m (Ref. 3). The NBD of different chains interact with each other (black arrows), possibly contributing to the stabilization of the large distance between the NBDs of a given chain. B: Sav1866 of *Staphylococcus aureus*, PDB ID: 2hyd (Ref. 10). The TMD of proteins in neighboring cells interact with each other (black arrows) and possibly stabilize the outward-open state (green arrow). Different colors are used to distinguish the different chains.

Table S1. Summary of the experimental conformations observed for different ABC transporters, including Sav1866 (PDB: 2hyd)[10], MsbA (PDB: 3b5w, 3b5x, 3b5z, 3b60)[2,11], McjD (PDB: 4pl0)[12], PglK (PDB: 5c73, 5c76, 5c78)[5], Pgp (PDB: 4m1m)[13], CmABCB1 (PDB: 3wme)[4], ABCB10 (PDB: 3zdq, 4ayw)[14] and BmrCD[11]. The conformation of the TMD is described by its level of opening on the intracellular side (intracel conform) and extracellular side (extracel conform). It is read directly from the X-ray structures or deduced from DEER measurements. Distances reported for the X-ray structures are taken between residues corresponding to those used for DEER measurements in BmrCD. 2AMP-PNP, a homolog for the pre-hydrolysis state, is assumed to correspond to the 2ATP state in simulations. ADP-vanadate, a homolog of the post-hydrolysis state[15] is assumed to correspond to the ATP/ADP state in the simulations[16].

Transporter (Method)	Equivalent amino acids	1 ADP/Vi (ATP/ADP)	Extracel conform	Intracel conform	2 AMP-PNP (2 ATP)	Extracel conform	Intracel conform	2 ADP	Extracel conform	Intracel conform	2 Apo	Extracel conform	Intracel conform	Ref.	PDB ID
		Dist. [Å]			Dist. [Å]			Dist. [Å]			Dist. [Å]				
Sav1866 (X-ray)	63 / 63	-	-		42.4	open		43.7	open		-	-		10,17	2hyd 2onj
	99 / 99	-		-	34.3		closed	34.3		closed	-		-		
MsbA (X-ray)	158 / 158	44.8	open		43.5	open		-	-		42.8; 41.2	closed; closed		2	3b5w 3b5x 3b5z 3b60
	103 / 103	35		closed	32.2		closed	-		-	42.5; 74.2		closed; open		
McjD (X-ray)	79 / 79	-	-		22.2	closed		-	-		-	-		12	4pl0
	110 / 110	-		-	31.4		closed	-		-	-		-		
PglK (X-ray)	75 / 75	-	-		-	-		42	closed		38.2; 40.7	closed; closed		5	5c73 5c76 5c78
	111 / 111	-		-	-		-	32.4		closed	66.2; 61		open; open		
Pgp (X-ray)	111 / 758	-	-		-	-		-	-		34.7	closed		13	4m1m
	146 / 787	-		-	-		-	-		-	50.7		open		
CmABCB1 (Xray)	168 / 168	-	-		-	-		-	-		33.7	closed		4	3wme
	199 / 199	-		-	-		-	-		-	44.9		open		
ABCB10 (X-ray)	216 / 216	-	-		40.1	closed		-	-		41	closed		14	3zdq 4ayw
	250 / 250	-		-	47.6		open			-	47.9		open		

MsbA (DEER)	158 / 158	50; 70	open; open		50; 70	open; open		-	-		38	closed		11	
	103 / 103	47; 77		closed; open	47; 77		closed; open	-		-	77; 47		open; closed		
BmrCD (DEER) in micelles	55 / 146	63; 37, 42	open; closed		37, 42	closed		37, 42	closed		37, 42	closed		11	
	96 / 188	47; 60		closed; open	60; 47		open; closed	60; 47		open; closed	60		open		
TM287/288 (DEER) in micelles	50 / 271	> 30	open		< 30	closed		<30	closed		< 30	closed		18	
	350 / 475	< 30		closed	< 30; > 30 * *ATP-EDTA		closed; open	<30		closed	< 30		closed		
Sav1866 (MD)	63 / 63	43	open		36	closed		35	closed		35	closed		This work	
	99 /99	37		closed	35		closed	35		closed	35		closed		
Total no. of conformations (X-ray, DEER)			**4**	**4**		**7**	**7**		**4**	**4**		**10**	**10**		
Conform. in agreement with MD / Total no. of conformations			**4 / 4**	**4 / 4**		**4 / 7**	**5 / 7**		**3 / 4**	**3 / 4**		**10 / 10**	**2 / 10**		

Table S2. Helical segments used for the analysis of rotation angles in helices 1 and 6

Helix	Segments used for vector definition	Segment used for alignment
1	u: 1-11 m: 12-26	m,t: 12-34
6	u: 277-290 m: 291-300	m,t: 291-308

Table S3. Helical segments used for the analysis of kink angles in helices 3 and 4

Helix	Segments used for vector definition
3	u: 140-158 m: 126-137
4	u: 161-180 m: 183-208

References

(1) Xu, Y.; Egido, E.; Li-Blatter, X.; Müller, R.; Merino, G.; Bernèche, S.; Seelig, A. Allocrite Sensing and Binding by the Breast Cancer Resistance Protein (ABCG2) and P-Glycoprotein (ABCB1). *Biochemistry* **2015**, *54*, 6195-6206.

(2) Ward, A.; Reyes, C. L.; Yu, J.; Roth, C. B.; Chang, G. Flexibility in the ABC transporter MsbA: Alternating access with a twist. *Proc Natl Acad Sci U S A* **2007**, *104*, 19005-19010.

(3) Aller, S. G.; Yu, J.; Ward, A.; Weng, Y.; Chittaboina, S.; Zhuo, R.; Harrell, P. M.; Trinh, Y. T.; Zhang, Q.; Urbatsch, I. L.; Chang, G. Structure of P-glycoprotein reveals a molecular basis for poly-specific drug binding. *Science* **2009**, *323*, 1718-1722.

(4) Kodan, A.; Yamaguchi, T.; Nakatsu, T.; Sakiyama, K.; Hipolito, C. J.; Fujioka, A.; Hirokane, R.; Ikeguchi, K.; Watanabe, B.; Hiratake, J.; Kimura, Y.; Suga, H.; Ueda, K.; Kato, H. Structural basis for gating mechanisms of a eukaryotic P-glycoprotein homolog. *Proc Natl Acad Sci U S A* **2014**, *111*, 4049-4054.

(5) Perez, C.; Gerber, S.; Boilevin, J.; Bucher, M.; Darbre, T.; Aebi, M.; Reymond, J. L.; Locher, K. P. Structure and mechanism of an active lipid-linked oligosaccharide flippase. *Nature* **2015**, *524*, 433-438.

(6) Verhalen, B.; Wilkens, S. P-glycoprotein retains drug-stimulated ATPase activity upon covalent linkage of the two nucleotide binding domains at their C-terminal ends. *J Biol Chem* **2011**, *286*, 10476-10482.

(7) Loo, T. W.; Bartlett, M. C.; Detty, M. R.; Clarke, D. M. The ATPase activity of the P-glycoprotein drug pump is highly activated when the N-terminal and central regions of the nucleotide-binding domains are linked closely together. *J Biol Chem* **2012**, *287*, 26806-26816.

(8) St-Pierre, J. F.; Bunker, A.; Róg, T.; Karttunen, M.; Mousseau, N. Molecular dynamics simulations of the bacterial ABC transporter SAV1866 in the closed form. *J Phys Chem B* **2012**, *116*, 2934-2942.

(9) Aittoniemi, J.; de Wet, H.; Ashcroft, F. M.; Sansom, M. S. Asymmetric switching in a homodimeric ABC transporter: a simulation study. *PLoS Comput Biol* **2010**, *6*, e1000762.

(10) Dawson, R. J.; Locher, K. P. Structure of a bacterial multidrug ABC transporter. *Nature* **2006**, *443*, 180-185.

(11) Mishra, S.; Verhalen, B.; Stein, R. A.; Wen, P. C.; Tajkhorshid, E.; Mchaourab, H. S. Conformational dynamics of the nucleotide binding domains and the power stroke of a heterodimeric ABC transporter. *Elife* **2014**, *3*, e02740.

(12) Choudhury, H. G.; Tong, Z.; Mathavan, I.; Li, Y.; Iwata, S.; Zirah, S.; Rebuffat, S.; van Veen, H. W.; Beis, K. Structure of an antibacterial peptide ATP-binding cassette transporter in a novel outward occluded state. *Proc Natl Acad Sci U S A* **2014**, *111*, 9145-9150.

(13) Li, J.; Jaimes, K. F.; Aller, S. G. Refined structures of mouse P-glycoprotein. *Protein Sci* **2014**, *23*, 34-46.

(14) Shintre, C. A.; Pike, A. C.; Li, Q.; Kim, J. I.; Barr, A. J.; Goubin, S.; Shrestha, L.; Yang, J.; Berridge, G.; Ross, J.; Stansfeld, P. J.; Sansom, M. S.; Edwards, A. M.; Bountra, C.; Marsden, B. D.; von Delft, F.; Bullock, A. N.; Gileadi, O.; Burgess-Brown, N. A.; Carpenter, E. P. Structures of ABCB10, a human ATP-binding cassette transporter in apo- and nucleotide-bound states. *Proc Natl Acad Sci U S A* **2013**, *110*, 9710-9715.

(15) Oldham, M. L.; Chen, J. Snapshots of the maltose transporter during ATP hydrolysis. *Proc Natl Acad Sci U S A* **2011**, *108*, 15152-15156.

(16) Urbatsch, I. L.; Sankaran, B.; Bhagat, S.; Senior, A. E. Both P-glycoprotein nucleotide-binding sites are catalytically active. *J Biol Chem* **1995**, *270*, 26956-26961.

(17) Dawson, R. J.; Locher, K. P. Structure of the multidrug ABC transporter Sav1866 from Staphylococcus aureus in complex with AMP-PNP. *FEBS Lett* **2007**, *581*, 935-938.

(18) Timachi, M. H.; Hutter, C. A.; Hohl, M.; Assafa, T.; Böhm, S.; Mittal, A.; Seeger, M. A.; Bordignon, E. Exploring conformational equilibria of a heterodimeric ABC transporter. *Elife* **2017**, *6*, e20236.